Available online at www.sciencedirect.com
ScienceDirect
Tetrahedron 62 (2006) 11916–11924
Tetrahedron

Density functional theory calculations and experimental parameters for mutarotation of 6-deoxy-L-mannopyranosyl hydrazine

Mabel Fragoso-Serrano,[a] Rogelio Pereda-Miranda[a] and Carlos M. Cerda-García-Rojas[b,*]

[a]*Departamento de Farmacia, Facultad de Química, Universidad Nacional Autónoma de México, Ciudad Universitaria, Mexico City 04510, Mexico*
[b]*Departamento de Química, Centro de Investigación y de Estudios Avanzados del Instituto Politécnico Nacional, Apartado 14-740, Mexico City 07000, Mexico*

Received 2 August 2006; revised 21 September 2006; accepted 22 September 2006
Available online 25 October 2006

Abstract—The geometry and energy profiles of the mutarotation pathway present in the equilibrium of 6-deoxy-β-L-mannopyranosyl 2,4-dinitrophenylhydrazine (**1a**), 6-deoxy-L-mannose 2,4-dinitrophenylhydrazone (**1b**), and 6-deoxy-α-L-mannopyranosyl 2,4-dinitrophenylhydrazine (**1c**) were modeled by DFT calculations at B3LYP/6-31G(d) level affording ΔG_{DFT}=0.000 kcal/mol, ΔG_{DFT}=0.174 kcal/mol, and ΔG_{DFT}=3.411 kcal/mol, respectively. Experimentally, the β-L-pyranose **1a** occurs in 50% followed by the acyclic structure **1b** in 44% as well as by the α-L-anomer **1c** in 6%. The conformations of **1a–c** and their corresponding 2,3,4-triacetyl derivatives **2a–c** were studied by molecular modeling and NMR spectroscopy. IR frequencies, NMR chemical shifts, and X-ray diffraction analysis were employed to compare theoretical with experimental structural parameters.

1. Introduction

Hydrazine derivatives play very important roles in agriculture, pharmaceutical, and chemical industries, and in many aspects of several emerging technologies.[1] This wide class of substances has attracted the attention of both synthetic[2] and theoretical chemists[3] because they represent relevant models for reactivity exploration and the study of the conformational behavior of nitrogen-containing substances. Combination of hydrazine compounds with sugars affords glycosylhydrazine derivatives, which increase the complexity of the chemical structure and properties of the hydrazine moiety. An interesting aspect of glycosylhydrazines, in particular of glycopyranosylhydrazines (e.g., **1a**), is their ability to establish an equilibrium with the corresponding acyclic glycosylhydrazones (**1b**), which leads to the anomeric form of the cyclic glycopyranosylhydrazines (e.g., **1c**) as exemplified in Scheme 1. This equilibrium can be studied under terms comparable to those of sugars mutarotation.[4]

There is no fully delineated systematization that can explain and predict the equilibrium for glycosylhydrazine derivatives. It seems to depend on the structure and stereochemistry of each particular carbohydrate as well as on the acidity or basicity of the solution.[5,6] The mutarotational process has been often described as a tautomerism[6] because of the prevalence of the equatorial *N*-glycosidic anomer and the open chain glycosylhydrazone components, both over that of the anomer carrying the *N*-moiety axially oriented (e.g., **1a** and **1b** over **1c**). In several hydrazine derivatives, particularly for those of rhamnose and mannose, it has also been proved that the predominant isomer in the crystalline state[7–9] is not always the one observed in solution.[5,6,10]

A major part of our ongoing research is directed toward the application of molecular modeling in the stereochemical and conformational elucidation of polyoxygenated molecules derived from 6-deoxyhexoses.[11,12] A theoretical methodology to model and predict the mutarotational equilibrium among the β-L-anomer **1a**, the acyclic component **1b**, and the α-L-anomer **1c** is described and compared to the results obtained by NMR data. The geometric and energetic mutarotational pathways were analyzed by density functional theory calculations at B3LYP/6-31G(d) level.[13] In addition, the same protocols were applied to study the structure and conformation of acetyl derivatives **2a–c** and **3**. Although theoretical approaches on the structure of monosaccharides[4,14–16] and glycopyranosylamines[17] have

Keywords: Glycosylhydrazines; Mutarotation; DFT calculations; NMR; X-ray analysis.
* Corresponding author. Tel.: +52 55 5061 3800x4035; fax: +52 55 5747 7137; e-mail: ccerda@cinvestav.mx

0040–4020/$ - see front matter © 2006 Elsevier Ltd. All rights reserved.
doi:10.1016/j.tet.2006.09.090

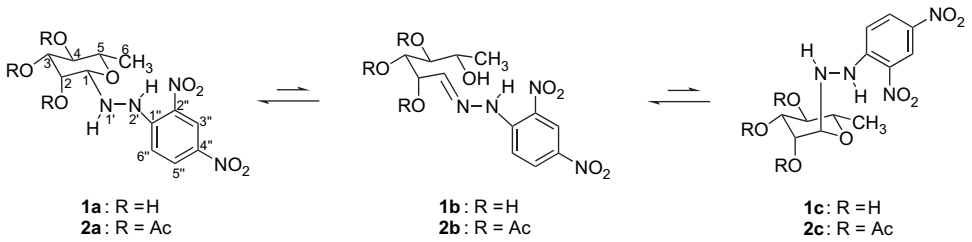

1a: R =H
2a: R = Ac

1b: R =H
2b: R = Ac

1c: R =H
2c: R = Ac

Scheme 1. Mutarotation in glycosylhydrazine derivatives.

recently been published, there are as yet no DFT structural and mutarotational analyses of glycosylhydrazine derivatives.

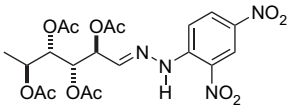

3

2. Results and discussion

6-Deoxy-L-mannose (L-rhamnose) treated with 2,4-dinitrophenylhydrazine produced, after crystallization in EtOH, the stable cyclic 1-(6-deoxy-β-L-mannopyranosyl)-2-(2,4-dinitrophenyl) hydrazine (**1a**) with a molecular formula of $C_{12}H_{16}N_4O_8$. Its melting point (165–167 °C) surprisingly matched that previously reported for hydrazone **1b**.[18] However, NMR analysis supported our suspicion that the reported open chain substance is in fact the β-L-pyranose **1a**. The signal for the anilinic NH was recorded at δ 9.65 (s) while the glycosidic NH was registered at δ 5.78 and shown to be coupled with the anomeric proton H-1 at δ 4.16 (*trans*-diaxial coupling constant $J_{NH,1}$=11.5 Hz) in the ^{1}H NMR spectrum in DMSO-d_6. The ^{13}C NMR spectrum was also consistent with that for the pyranoside structure for **1a**, e.g., the anomeric carbon C-1 at δ 87.0. On addition of trace amounts of hydrochloric acid, the DMSO-d_6 solution of **1a** immediately produced a mixture of four major components detectable through their anilinic NH protons at δ 9.66, 9.67, 11.39, and 12.78 in the ^{1}H NMR corresponding to the β-L-anomer **1a**, the α-L-anomer **1c**, and the acyclic component **1b** in its *E* and *Z*-configurations at the C=N double bond, respectively (Scheme 2). The percentage of the isomers **1a** (50%), **1b**-*E* (36%), **1b**-*Z* (8%), and **1c** (6%) was calculated by the signal integrals of selected hydrogen atoms as can be seen in Figure 1. Structural assignments were confirmed through the signals for the anomeric carbon atoms at δ 87.0 for **1a** and 87.9 for **1c**, the signals for the C-1 sp^2 carbon atoms at δ 155.7 for **1b**-*E* and δ 152.9 for **1b**-*Z*. These assignments were further confirmed through a detailed analysis of the 2D NMR spectra of the mutarotational equilibrated mixture, which included COSY, NOESY, gHSQC, and gHMBC experiments. NOESY spectrum was particularly useful in confirming the double bond geometry in the **1b**-*E* and **1b**-*Z*-isomers because of the strong interaction between the anilinic NH and the vinylic H-1 signals only observed in **1b**-*E* but not in **1b**-*Z*. The information provided by the COSY, gHSQC, and gHMBC spectra allowed the individual assignment of signals for the equilibrium components, including the anomeric protons for **1a** and **1c** at δ 5.78 and 4.52, respectively, and the vinylic protons for **1b**-*E* and **1b**-*Z* at δ 8.03 and 7.22, respectively. The interconversion between the α- and β-anomers was also registered by the change in the specific rotation of compound **1a** in acidic solution.

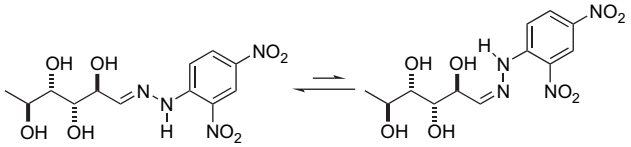

1b-*E* **1b**-*Z*

Scheme 2. *E*-*Z* Isomerization of **1b**.

In order to study the structures of the acyclic components and the α-L-pyranoside form, it was necessary to produce substances that could be isolated for spectroscopic analysis by NMR. Treating pure **1a** with acetic anhydride in pyridine afforded the following such substances: 1-(2,3,4-tri-*O*-acetyl-6-deoxy-β-L-mannopyranosyl)-2-(2,4-dinitrophenyl)-hydrazine (**2a**), 2,3,4-tri-*O*-acetyl-6-deoxy-L-mannose 2,4-dinitrophenylhydrazone (**2b**), and 1-(2,3,4-tri-*O*-acetyl-6-deoxy-α-L-mannopyranosyl)-2-(2,4-dinitrophenyl)hydrazine (**2c**), together with 2,3,4,5-tetra-*O*-acetyl-6-deoxy-L-mannose 2,4-dinitrophenylhydrazone (**3**). Additionally, treatment of **1a** with acetyl chloride afforded **3** as the main product. Compounds **2a**, **2b**, and small amounts of **2c** were purified by normal phase HPLC. However, they equilibrated to the original mixture (**2a**–**c**) after standing for 24 h in individual acidic $CDCl_3$ solutions. Linear derivative **2b** was obtained exclusively in its *E*-configuration.

The ^{1}H NMR spectrum of **2a** clearly indicated the presence of a pyranoside ring bearing three acetoxyl substituents. In this case, the signal for the anilinic NH appeared at δ 9.63 while the NH attached to the saccharide was at δ 4.52 and strongly coupled with the anomeric proton H-1 at δ 4.40 ($J_{NH,1}$=11.4 Hz). Adding D_2O permitted the assignment of the labile hydrogen atoms. ^{13}C NMR spectrum exhibited the characteristic signal for the C-1 anomeric carbon at δ 85.7. The X-ray diffraction analysis of **2a** confirmed the structure and stereochemistry of this substance (Fig. 2), which exhibited the 2,4-dinitrophenylhydrazine moiety in a β-equatorial orientation at C_1. The hydrogen atoms H_1–H_2 and H_2–H_3 of this 6-deoxymannose derivative (**2a**) were found in a *syn*-clinal relationship while H_3–H_4 and H_4–H_5 appeared in an *anti*-periplanar orientation (Table 1). The pyranoside ring exists in a conformation close to the classical chair, slightly distorted toward a twist-boat.

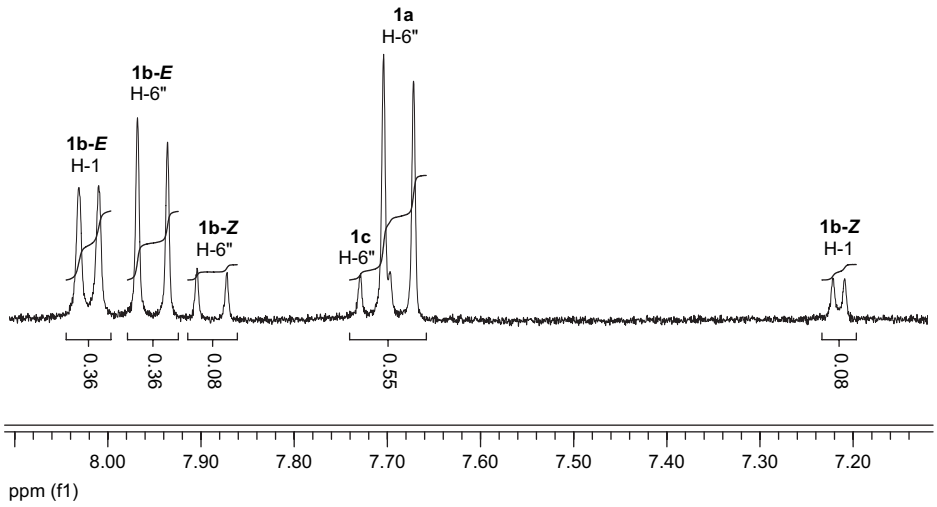

Figure 1. A section of the ^{1}H NMR aromatic region (δ 8.10–7.12) for the equilibrated mixture of 1-(6-deoxy-β-L-mannopyranosyl)-2-(2,4-dinitrophenyl)hydrazine (**1a**), 6-deoxy-L-mannose 2,4-dinitrophenylhydrazone (**1b**, *E* and *Z*-isomers), and 1-(6-deoxy-α-L-mannopyranosyl)-2-(2,4-dinitrophenyl)hydrazine (**1c**) in DMSO-d_6+HCl at 300 MHz.

Density functional theory calculations were used to analyze the minimum energy pathway and the geometry of each component in the mutarotational equilibrium (Scheme 1). Conformational distribution of compounds **1a**–**c** and **2a**–**c** was individually calculated by molecular mechanics (MMFF) through an extensive Monte Carlo random search.[19] Due to the presence of the hydrazine moiety, the conformational analysis of the pyranoside rings of **1a**, **1c**, **2a**, and **2c** was far more complicated than that expected for simple hexose derivatives. However, in the absence of the usual hydroxymethyl group, normally prominent in the conformational properties of glucopyranosides, the difficulties involved in this analysis were mitigated.[15] A molecular mechanics energy range of 0–10 kcal/mol was selected for these calculations, which yielded a total of 30, 106, and 63 minimum energy conformations for compounds **1a**, **1b**, and **1c**, respectively. Low-energy conformations were correlated to the rotations of the C_1–N_1–N_2–$C_{1'}$ bonds, which defined the conformation of the dinitrophenylhydrazine moiety. The cooperative clockwise or counterclockwise orientations of the hydroxyl groups also played a relevant role in the conformational distribution. Each conformational species was geometry analyzed and selected according to the maximum number of cooperative hydrogen bonds. Using this filtering criteria, 7, 27, and 10 conformations for **1a**, **1b**, and **1c**, respectively, were optimized by DFT calculations employing the B3LYP method with the 6-31G(d) basis set. To ensure a full exploration of the conformational space in linear derivative **1b**, the distribution was additionally calculated through a systematic search model[11] of 54 conformational variants resulting from rotation of the C_2–C_3, C_3–C_4, and C_4–C_5 bonds every 120°, as well as the C_1–C_2 bond by 180°. The minimum energy structures were optimized by DFT calculations by employing the same method and basis set to yield similar results as those obtained from the Monte Carlo method, also within a 0–10 kcal relative range. Analysis of the molecular geometry of each conformer revealed that the physical principles that govern the conformational distribution can be mainly defined by the presence of an intramolecular hydrogen bond patterns as well as steric effects and repulsive 1,3 oxygen–oxygen interactions. Table 2 contains the 27 refined global and local minimum energy structures ordered according to their stability and the corresponding H–C–C–H dihedral angles found in the C_1–C_2–C_3–C_4–C_5 fragment of **1b**. Each rotameric species was named by using the following descriptors: *P* for plus (ca. +60°), *A* for anti (ca.+180°), and *M* for minus (ca. −60°) according to the nearest value for the measured dihedral angles.

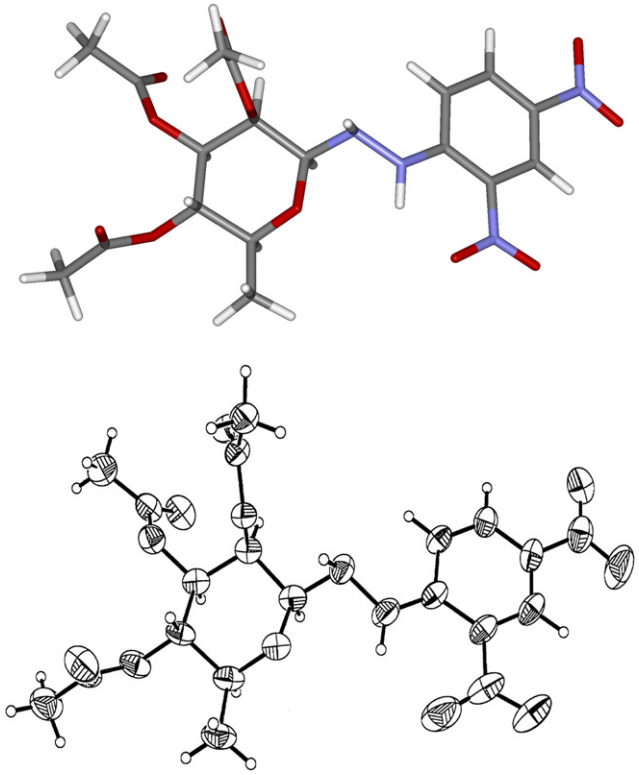

Figure 2. Comparison between the DFT B3LYP/6-31G(d) molecular model of **2a** and its X-ray structure.

Figure 3 illustrates the DFT minimum energy pathway for the mutarotational process from **1a** to **1c** involving six key acyclic conformers of **1b** in the *E*-configuration. The

Table 1. DFT B3LYP/6-31G(d) dihedral angles (in deg) and calculated[a] versus observed[b] ^1H–^1H vicinal coupling constants (in hertz) for the global minimum of pyranosides **1a**, **1c**, **2a**, and four conformations of **2c** (comparison between DFT and X-ray dihedral angles for **2a** is shown)

Compound	$\phi_{H1-C-C-H2}$	$J_{1,2(calcd)}$	$J_{1,2(obsd)}$	$\phi_{H2-C-C-H3}$	$J_{2,3(calcd)}$	$J_{2,3(obsd)}$	$\phi_{H3-C-C-H4}$	$J_{3,4(calcd)}$	$J_{3,4(obsd)}$	$\phi_{H4-C-C-H5}$	$J_{4,5(calcd)}$	$J_{4,5(obsd)}$
1a	−54.1	1.3	0.6	51.2	3.4	3.0	−176.3	9.4	9.3	179.3	9.2	9.2
1c	70.8	1.7	2.0	53.7	3.0	3.3	−172.8	9.1	9.1	177.7	9.2	9.0
2a[c]	−55.0 (−49.3)	1.4	1.2	54.0 (53.5)	3.1	3.3	−173.0 (−174.4)	9.4	10.2	176.0 (−175.3)	9.2	9.3
2c-1	71.3	2.4	—	56.1	4.5	—	−173.0	9.4	—	173.4	9.1	—
2c-2	103.7	1.5	—	59.6	4.1	—	−163.8	8.2	—	116.9	2.8	—
2c-3	168.1	8.4	—	−51.1	5.2	—	−64.7	3.3	—	73.6	1.3	—
2c-4	166.0	8.2	—	−58.3	4.2	—	−103.2	0.6	—	163.2	8.6	—
2c-avg		5.1[d]	4.1		4.5[d]	5.8		5.4[d]	5.0		5.5[d]	6.9

[a] Calculated from DFT dihedral angles via a generalized Karplus-type equation.
[b] Measured in DMSO for **1a** and **1c** and in $CDCl_3$ for **2a** and **2c**.
[c] X-ray dihedral angles are shown in parenthesis.
[d] Averaged value.

β-L-anomer (**1a**) is mainly found in a single conformation with cooperative anticlockwise orientation of the hydroxyl groups and a *trans*-diaxial orientation of the H_1–C_1–N_1–H moiety. For the open chain component **1b**, conformer **1b**-***MPAA***, illustrated, is generated by the pyranoside ring opening at the C_1–O_5 bond of **1a**. The population of this highly energetic conformer (E_{rel}=10.932 kcal/mol) moves toward the more stable rotamer **1b**-***PPPP***, which is in fact the predominant species for the linear component **1b** and contains four optimally-oriented cooperative hydrogen bonds in the tetrahydroxylated chain. However, the rotameric population is distributed to generate an equilibrium involving small amounts of **1b**-***PPPA*** and **1b**-***PPAA***, which ultimately leads to the α-L-anomer **1c**. The rotameric species of **1b** that are not depicted in Figure 3 but listed in Table 2 are also present in the equilibrium according to the Boltzmann distribution, and can be located in branches derived from the main pathway for the mutarotational process. In the α-form, the global minimum **1c** (E_{DFT}=−1287.454180 au, Fig. 3) was followed by a second one (E_{DFT}=−1745.451136 au) arising from the pyranoside chair inversion at the point where the hydrazine moiety and the hydroxyl group at C-2 adopted an equatorial orientation. In this minimum energy conformer, the methyl group at C-5 and the hydroxyl groups at C-3 and C-4 remained axially oriented. This conformational inversion was further studied with peracetylated derivative **2c**.

Table 1 lists the H–C–C–H torsion angles of the global minimum for the cyclic substances **1a** (E_{DFT}=−1287.460165 au) and **2a** (E_{DFT}=−1745.459742 au), both of which showed a prevalent conformation. In contrast, a complex rotameric equilibrium was established in triacetylated derivative **2b** in a similar way as that previously found

Table 2. DFT global and local minimum energy conformers and selected H–C–C–H dihedral angles for the acyclic component **1b**

Conformer[a]	E_{DFT}[b]	E_{rel}[c]	H_1–H_2[d]	H_2–H_3[d]	H_3–H_4[d]	H_4–H_5[d]
1b-*PPPP*	−1287.454425	3.602	81.9	55.5	53.2	51.7
1b-*MPPP*	−1287.453216	4.360	−51.5	53.2	53.9	52.3
1b-*MAMA*	−1287.449155	6.909	−62.7	172.5	−68.9	174.1
1b-*MAPP*	−1287.449031	6.987	−59.2	−176.8	71.7	59.3
1b-*PAAA*	−1287.446925	8.308	77.4	−178.2	177.8	−161.6
1b-*PMPA*	−1287.446698	8.451	80.0	−50.4	83.6	−174.1
1b-*PPPA*	−1287.446668	8.469	72.7	58.8	77.4	−175.5
1b-*MAPM*	−1287.446631	8.493	−62.5	−178.9	80.5	−51.3
1b-*AMPP*	−1287.446391	8.644	167.5	−60.6	54.2	57.7
1b-*PPMP*	−1287.446275	8.716	63.5	64.1	−63.7	56.2
1b-*PPPM*	−1287.445829	8.996	80.6	60.0	59.9	−57.7
1b-*MAAP*	−1287.445533	9.182	−62.3	−168.7	−175.7	85.1
1b-*MAAM*	−1287.445347	9.299	−61.8	−175.9	174.1	−52.7
1b-*PAMP*	−1287.445205	9.388	81.7	164.4	−71.5	47.4
1b-*PPAA*	−1287.444489	9.837	84.4	77.5	−172.6	−165.2
1b-*MPPA*	−1287.444379	9.906	−53.2	53.2	72.7	−177.0
1b-*AMAM*	−1287.443931	10.187	175.2	−54.5	179.7	−53.7
1b-*MAPA*	−1287.443230	10.627	−62.0	173.2	71.7	−177.6
1b-*MPAA*	−1287.442744	10.932	−41.3	80.8	−169.7	−165.2
1b-*AMAA*	−1287.442687	10.968	175.8	−56.0	173.2	−178.0
1b-*PMAP*	−1287.442280	11.223	55.9	−64.7	143.2	55.2
1b-*PPMA*	−1287.441215	11.891	54.4	69.1	−70.7	170.0
1b-*MPAP*	−1287.441208	11.896	−58.1	51.2	169.1	53.9
1b-*AMMA*	−1287.440794	12.156	174.9	−62.8	−64.5	169.8
1b-*AMPM*	−1287.439980	12.666	−161.8	−56.3	60.6	−58.5
1b-*APAA*	−1287.439708	12.837	177.5	52.3	139.5	177.6
1b-*MAMM*	−1287.439604	12.902	−57.3	169.5	−60.1	−62.8

[a] Descriptors are based on H–C–C–H dihedral angles ca. +60°(*P*), ca. 180°(*A*), and ca. −60°(*M*) for the C_1–C_2–C_3–C_4–C_5 fragment.
[b] DFT B3LYP/6-31G(d) total energy in au.
[c] Relative DFT energies (kcal/mol) are in reference to **1a** (E_{DFT}=−1287.460165 au; 1 au=627.51 kcal/mol).
[d] H–C–C–H dihedral angle.

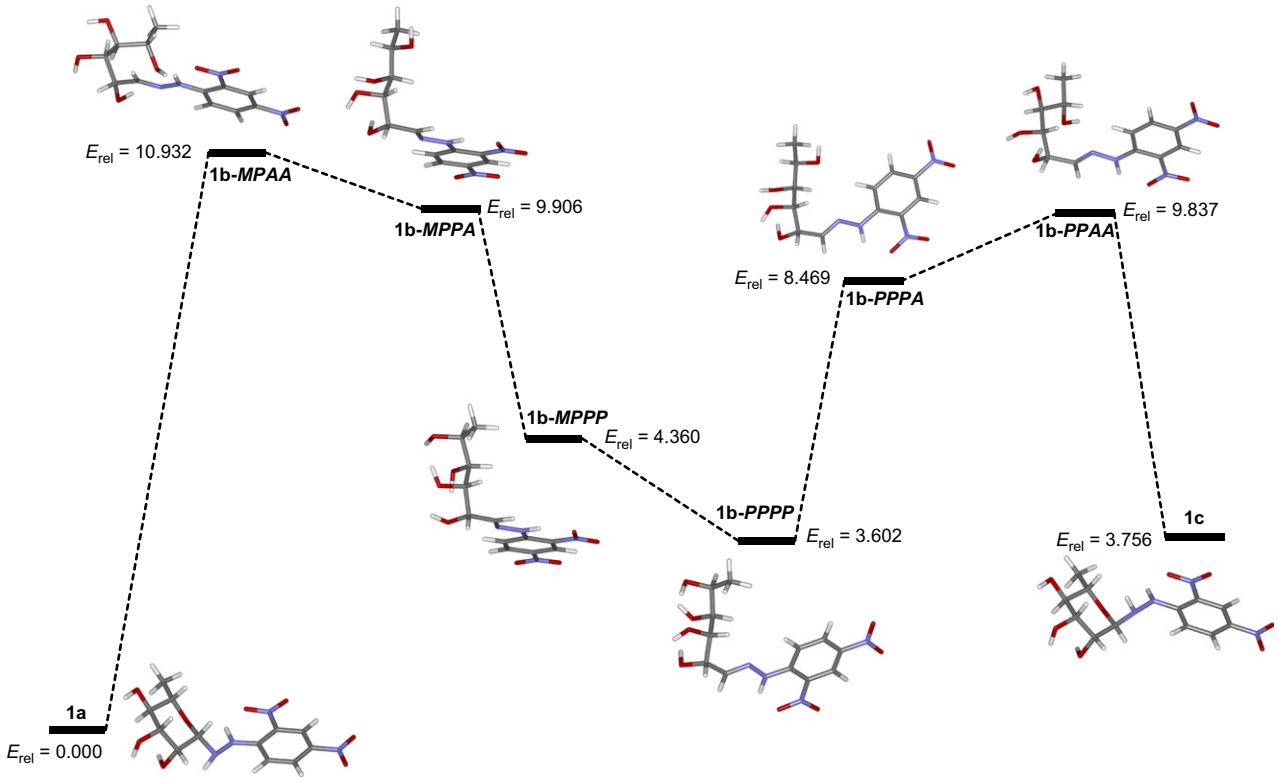

Figure 3. DFT B3LYP/6-31G(d) minimum energy pathway for the mutarotational process from **1a** to **1c**. Relative energies are in kcal/mol referred to the global minimum **1a**.

for tetra-*O*-acetyl-6-deoxy-L-mannose derivatives.[11] This resemblance became evident from the $J_{2,3}$=8.5, $J_{3,4}$=1.9, and $J_{4,5}$=8.5 Hz coupling constant values, which remained very close in all the linear substances derived from this carbohydrate. For pyranoside **2c**, ring inversion occurred between the two possible chair conformations (**2c**-**1** and **2c**-**3**) through two low-energy twisted-boat conformations (**2c**-**2** and **2c**-**4**) as depicted in Figure 4. The equilibrium between the four conformations in **2c** (**2c**-**1**: E_{DFT}= −1745.452419 au; **2c**-**2**: E_{DFT}=−1745.451391 au; **2c**-**3**:

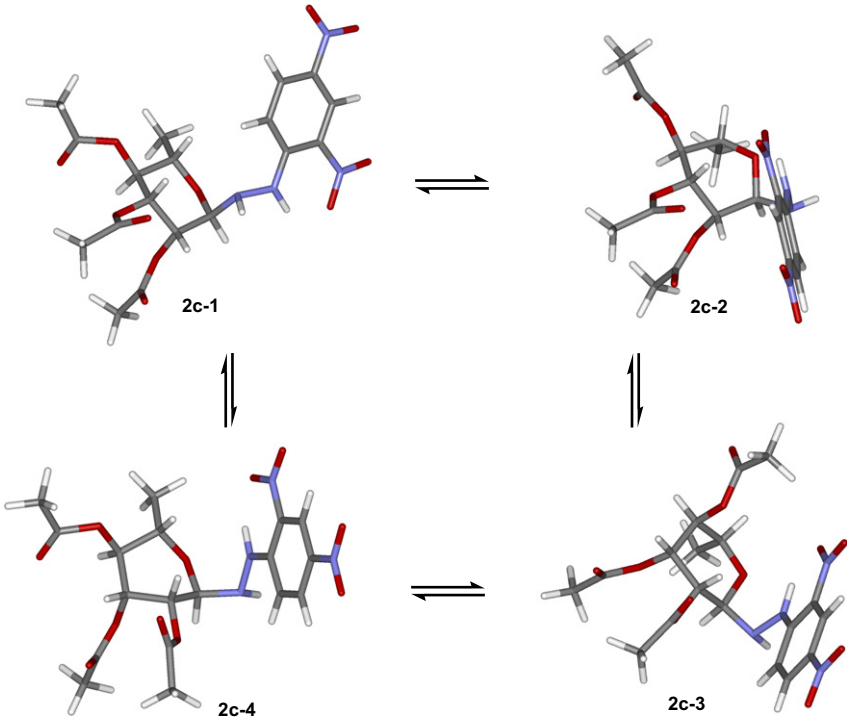

Figure 4. The conformational equilibrium of **2c**.

Table 3. DFT B3LYP/6-31G(d) conformation for the O–C1–C2–C3–C4–C5 rings of **1a**, **1c**, **2a**, and **2c**

Compound	Conformational contributions[a]			Ring conformation	Conformational parameters		
	Chair	Boat	Twist-boat		Q[b]	ϕ[c]	θ[c]
1a[d]	88	2	10	Between chair and half-chair	0.593	24.20	7.75
1c[d]	94	3	3	Distorted chair	0.556	22.88	3.19
2a[d]	93	0	6	Distorted chair	0.545	28.47	4.13
2a[e]	89	9	2	Distorted chair	0.583	4.42	6.77
2c-1[d]	91	6	3	Distorted chair	0.545	19.34	5.26
2c-2[d]	4	61	35	Between boat and twist-boat	0.709	10.73	87.58
2c-3[d]	96	1	3	Chair	0.511	22.53	2.46
2c-4[d]	1	59	40	Between boat and twist-boat	0.731	12.03	89.29

[a] Quantitative contributions of basic conformations in percentage.
[b] Total puckering amplitude in Å.
[c] In degrees.
[d] From density functional theory coordinates.
[e] From X-ray diffraction coordinates.

E_{DFT}=−1745.455161 au; and **2c-4**: E_{DFT}=−1745.451046 au) was detectable from the averaged experimental coupling constants ($J_{1,2}$=4.1, $J_{2,3}$=5.8, $J_{3,4}$=5.0, and $J_{4,5}$=6.9 Hz) measured by spectral simulation. The calculated ^{1}H NMR couplings constants for the four conformations (**2c-1** to **2c-4**) and the averaged values are listed in Table 1. In this equilibrium, the contributing factors to achieve the stability of conformer **2c-3** over **2c-1** were the equatorial orientation of the hydrazine moiety at C_1, the largest group attached to the six-membered ring; the interaction between the hydrogen atom at $N_{1'}$ and the oxygen atom of the pyranoside ring O_1 in the O_1–C_1–$N_{1'}$–H fragment (distance=2.53 Å) and the interaction between the hydrogen atom attached to $N_{2'}$ and the oxygen atom O_1 in the fragment O_1–C_1–$N_{1'}$–$N_{2'}$–H (distance=2.28 Å).

Cremer and Pople polar set of parameters[20] were calculated using the DFT and X-ray coordinates for the quantitative conformational description of the pyranoside minimum energy structures (Table 3). The Altona equation was used to convert dihedral angles into calculated vicinal coupling constants ($^3J_{H-H}$).[21] Calculated and observed ^{1}H–^{1}H vicinal coupling constants showed a good correlation, which validated the DFT conformations for the rigid compounds **1a** and **2a**, and for the mobile pyranoside **2c** (Table 1).

If only the relative DFT energy values of the structures in mutarotation were considered (Fig. 3), the prevalent component according to the Boltzmann distribution would be **1a**. However, by taking into account the thermodynamic factors, a better prediction of the mutarotation composition at the equilibrium was obtained. Table 4 presents the data obtained by a thermochemical analysis in which the corresponding vibrational frequencies and thermal parameters were calculated using the optimized B3LYP/6-31G(d,p) global minimum structures of **1a**, **1b**, and **1c**. The calculated frequencies were scaled by a factor of 0.97 and compared with the experimental frequencies measured in the IR spectrum of the mixture of **1a**, **1b**, and **1c** at equilibrium. Figure 5 shows good agreement between the calculated and observed values, validating the B3LYP/6-31G(d,p) thermodynamic parameters for the mutarotational components. These values were used for estimation of the relative populations of **1a**, **1b**-***PPPP***, and **1c** according to the Gibbs free energy equation $\Delta G=\Delta H-T\Delta S$ and $\Delta G=-RT\ \ln K$. These refined calculations for the three main components also considered the zero-point correction, and the thermal correction to energy and enthalpy, providing more accurate values than those reflected by the relative E_{DFT}. The ΔG values were estimated as ΔG_{DFT}=0.000 kcal/mol for **1a**, ΔG_{DFT}= 0.174 kcal/mol for **1b**-***PPPP***, and ΔG_{DFT}=3.411 kcal/mol for **1c**, which yielded a predicted population at equilibrium of 57.2%, 42.6%, and 0.2% for each species, respectively. These theoretical results were in line with the 50%, 44%,

Table 4. Thermochemical parameters (in kcal/mol) and population (in %) for the mutarotational equilibrium calculated with the B3LYP/6-31G(d,p) global minimum structures of **1a–c**

	ΔE_0[a]	ΔE_{298}[b]	ΔH_{298}[b]	ΔS_{298}[b]	ΔG_{298}[b]	p[b]
1a	0.000	0.000	0.000	0.000	0.000	57.2
1b	1.035	1.462	0.4463	1.734	0.174	42.6
1c	3.591	3.632	0.066	0.287	3.411	0.2

[a] Sum of electronic and zero-point energy.
[b] Calculated at 298.15 K and 1 atm. For the **1a** species the absolute values are E_0=−1287.18993 au, E_{298}=−1287.16810 au, H_{298}=24.890 kcal/mol, S_{298}=158.587 cal/mol K, and G_{298}=−1287.20379 au.

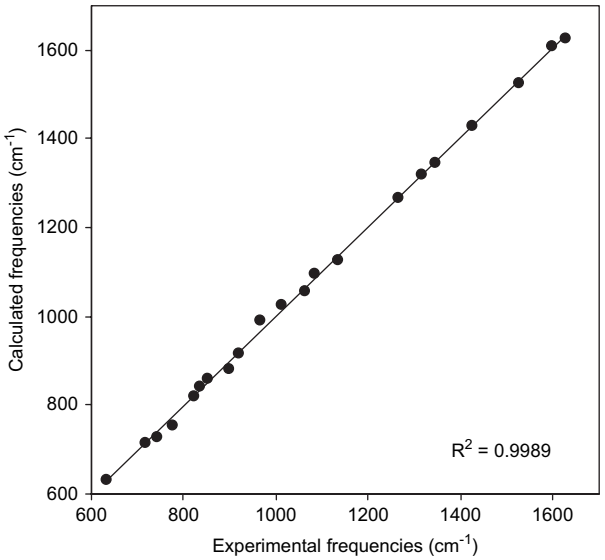

Figure 5. Comparison of the experimental infrared frequencies of compound **1a** with the corresponding calculated values obtained at the B3LYP/6-31G(d,p) level of theory.

Table 5. Comparison between theoretical and experimental ^{13}C NMR chemical shifts for **1a**

Atom	δ_{calcd} [a]	δ_{scaled} [b]	δ_{exp} [c]	$\lvert\delta_{scaled}-\delta_{exp}\rvert$
C-1′	135.1	145.3	149.0	3.7
C-4′	125.0	135.2	135.3	0.1
C-2′	118.7	128.9	128.3	0.6
C-5′	117.1	127.3	129.8	2.5
C-3′	112.2	122.4	123.2	0.8
C-6′	101.0	111.2	116.0	4.8
C-1	80.3	90.5	87.0	3.5
C-3	66.7	76.9	73.7	3.2
C-4	66.5	76.7	73.1	3.6
C-5	65.9	76.1	72.0	4.1
C-2	63.5	73.7	69.8	3.9
C-6	9.3	19.5	18.1	1.4

[a] Calculated at B3LYP/6-31G(d,p) level of theory using GIAO magnetic shielding.
[b] Calculated by linear fit of δ_{calcd} versus δ_{exp}.
[c] Measured at 300 MHz in DMSO-d_6 solution.

and 6% observed NMR ratio (Fig. 1). The entropic contribution, estimated as $\Delta S_{\mathbf{1a},\mathbf{1b}}$=5.814 cal/mol K and agreeing with the PM3 calculations for the mutarotation of glucopyranosylamine derivatives,[22] is notably important for the stability of acyclic structure **1b**. Finally, the experimental ^{13}C NMR chemical shifts for **1a** were compared with these obtained with isotropic magnetic shielding calculations using the SCF GIAO method at DFT/B3LYP level of theory and the basis set 6-31G(d,p). Diagnostic values for C-1 of each species were in close agreement with those obtained experimentally (Table 5).

3. Conclusions

DFT calculations, NMR analysis, and X-ray diffraction studies of 6-deoxy-L-mannopyranosyl hydrazine were performed in order to obtain conformational parameters. The DFT calculated values for the equilibrium among the mutarotational species **1a**, **1b**, and **1c** could be further refined by taking into consideration local conformers including all possible cooperative hydrogen bonded species and the inclusion of solvent modeling. Nevertheless, this work shows that DFT calculations at B3LYP/6-31G(d,p) level represent suitable tools to predict the thermodynamic properties, mutarotational composition, stereochemical features, and conformational preferences of glycosylhydrazines.

4. Experimental

4.1. General

Column chromatography was carried out with silica gel (70–230 mesh) Merck. $CDCl_3$ for NMR spectroscopy was filtered through dry alumina prior to use. HPLC separations were accomplished using an ISCO silica gel column (particle size: 10 μm; column size: 21.2 mm×250 mm) on a Waters (Milford, MA, USA) 600E multisolvent delivery system equipped with a Waters 410 refractive index detector connected to a computer (Optiflex 466/Dell). Control of the equipment, data acquisition, processing, and management of the chromatographic information was performed with the Millennium 2000 software program (Waters). IR spectra were determined on a Perkin–Elmer 16F PC or on a Buck 500 spectrophotometer. ORD was measured on a Perkin–Elmer 341 or JASCO DIP-360 polarimeters. The ^1H (300 MHz), ^{13}C (75.4 MHz), COSY, HMQC, and HMBC experiments were conducted on a Varian Mercury 300 spectrometer. LRMS were measured on a JEOL JMS-AX505HA mass spectrometer. HREIMS was determined on a Kratos concept II H mass spectrometer and HRFABMS were measured on a JEOL DX 300 mass spectrometer.

4.1.1. General procedures for recording the mutarotational equilibria. (a) NMR: solutions of pure samples (5 mg) of **1a** in DMSO-d_6 (0.8 mL) and **2a–c** in $CDCl_3$ (0.8 mL) or DMSO-d_6 (0.8 mL) were treated with 12.1 M HCl in H_2O (1 μL) in 5 mm NMR tubes. (b) Optical activity: specific rotation of a solution of **1a** (5 mg) in DMSO-d_6 (0.8 mL) was monitored at room temperature, $[\alpha]_D$ +35.0. Treatment of this solution with 12.1 M HCl in H_2O (1 μL) provoked an immediate decrease in the optical activity value, $[\alpha]_D$ +0.3. This rotation remained constant during the following 2 h.

4.1.2. pH measurements. The pH values were registered with a VWR Scientific pHmeter (model 8000). A mixture of DMSO-d_6 (4.8 mL) and H_2O (6 μL) has a pH 8.50. The pH of a mixture of compound **1a** (30 mg) in DMSO-d_6 (4.8 mL) and 12.1 M HCl in H_2O (6 μL) was 2.45 after 5 min of stirring while after 90 min it was 2.54. The acidity of the mixture was raised to pH 2.14 after addition of a second portion of HCl (6 μL).

4.1.2.1. (6-Deoxy-β-L-mannopyranosyl)-2-(2,4-dinitrophenyl)hydrazine (1a). A solution of 2,4-dinitrophenylhydrazine (0.3 g, 1.5 mmol) in sulfuric acid (0.5 mL) was added to a mixture of H_2O (2 mL) and EtOH (7 mL). The mixture was added to a solution of L-rhamnose monohydrate (0.5 g, 2.7 mmol) in EtOH (3 mL), left for 3 h at room temperature and 16 h at 4 °C. The product was crystallized as orange flakes, which were filtered, washed with 5% sodium bicarbonate solution and H_2O and then recrystallized from 90% EtOH in H_2O to afford **1a** (313 mg, 33%). Orange needles; mp 165–167 °C (lit.[18] 164–165 °C); IR (KBr) ν_{max} 3375, 1629, 1598, 1526, 1427, 1348, 1315, 1268, 1135, 1085, 1062, 1012, 968, 920, 900, 853, 835, 822, 777, 744, 718, 635 cm^{-1}; ORD (*c* 0.61, MeOH) $[\alpha]_{589}$ +34, $[\alpha]_{578}$ +37, $[\alpha]_{546}$ +39; ^1H NMR (300 MHz, DMSO-d_6) δ 9.65 (1H, br s), 8.83 (1H, d, *J*=2.5 Hz), 8.30 (1H, dd, *J*=9.6, 2.5 Hz), 7.68 (1H, d, *J*=9.6 Hz), 5.78 (1H, d, *J*=11.5 Hz), 5.01 (1H, d, *J*=4.9 Hz), 4.83 (1H, d, *J*=4.9 Hz), 4.81 (1H, d, *J*=5.2 Hz), 4.16 (1H, br d, *J*=11.5 Hz), 3.83 (1H, br t, *J*=4.5 Hz), 3.28 (1H, m), 3.18 (1H, m), 3.13 (1H, m), 1.20 (3H, d, *J*=5.7 Hz); ^{13}C NMR (75.4 MHz, DMSO-d_6) δ 149.0, 135.3, 129.8, 128.3, 123.2, 116.0, 87.0, 73.7, 73.1, 72.0, 69.8, 18.1; EIMS *m/z* (rel int.) $[M]^+$ 344 (1), $[M-C_4H_9O_3]^+$ 239 (8), 194 (11), $[239-NO_2]^+$ 193 (100), 184 (28), $[C_6H_5N_3O_4]^+$ 183 (43), 177 (21), 167 (15), 153 (28), 129 (26), 91 (21), 85 (29); HREIMS *m/z* 344.0957 (calcd for $C_{12}H_{16}N_4O_8$, 344.0968).

4.1.2.2. Acetylation of 1a. A solution of **1a** (100 mg) in pyridine (2.5 mL) was treated with acetic anhydride (2.5 mL) at room temperature for 24 h. The reaction mixture was worked-up[11] and the residue was purified by HPLC in

aliquots of 20 mg (*n*-hexane–EtOAc, 1:1, flow rate=6 mL/min) to yield **3** (23.3 mg, 15.7%, t_R=15.5 min), **2a** (50.0 mg, 36.6%, t_R=17.9 min), **2c** (1.6 mg, 1.2%, t_R=21.8 min), and **2b** (36.8 mg, 26.9%, t_R=26.8 min). Treatment of **1a** (100 mg) with acetyl chloride (5 mL) at room temperature for 2 h followed by evaporation under a N_2 flow and HPLC purification gave **3** in better yields (73 mg, 49%).

4.1.2.3. 1-(2,3,4-Tri-*O*-acetyl-6-deoxy-β-L-mannopyranosyl)-2-(2,4-dinitrophenyl)hydrazine (2a). Yellow prisms; mp 103–105 °C; IR ($CHCl_3$) ν_{max} 3751, 3365, 1750, 1620, 1594, 1524, 1429, 1372, 1339, 1311, 1238, 1226, 1060, 926, 836 cm^{-1}; ORD (*c* 1.29, $CHCl_3$) $[\alpha]_{589}$ +29, $[\alpha]_{578}$ +29, $[\alpha]_{546}$ +31; ^1H NMR (300 MHz, $CDCl_3$) δ 9.63 (1H, br s), 9.07 (1H, d, *J*=2.7 Hz), 8.27 (1H, dd, *J*=9.6, 2.7 Hz), 7.68 (1H, d, *J*=9.6 Hz), 5.62 (1H, dd, *J*=3.3, 1.2 Hz), 5.08 (1H, dd, *J*=10.2, 9.3 Hz), 5.00 (1H, dd, *J*=3.3, 10.2 Hz), 4.52 (1H, d, *J*=11.4 Hz), 4.40 (1H, dd, *J*=11.4, 1.2 Hz), 3.57 (1H, dq, 1H, *J*=9.3, 6.3 Hz), 2.23, 2.08, 2.00 (3H each, 3s), 1.32 (3H, d, *J*=6.3 Hz); ^{13}C NMR (75.4 MHz, $CDCl_3$) δ 170.1, 170.0, 169.8, 148.9, 137.3, 130.1, 129.7, 123.6, 115.6, 85.7, 72.1, 71.5, 70.1, 68.9, 20.7, 20.7, 20.5, 17.4; EIMS *m/z* (rel int.) $[M]^+$ 470 (4), 411 (2), 306 (9), 291 (10), 273 (17), 213 (8), 193 (9), 171 (20), 153 (73), 129 (11), 111 (69), 83 (25), $[C_2H_3O]^+$ 43 (100); HREIMS *m/z* 470.1270 (calcd for $C_{18}H_{22}N_4O_{11}$, 470.1285).

4.1.2.4. X-ray analysis of 2a. The crystal (0.22×0.25×0.46 mm) was obtained from EtOAc–hexane. It was monoclinic, space group *C*2, with *a*=21.017(2), *b*=8.154(2), *c*=13.591(2) Å, cell volume=2254.6 (7) $Å^3$, ρ_{calcd}=1.386 g/cm^3 for *Z*=4, MW=470.40, and *F*(000)e^-= 984. The intensity data were measured using Mo K_α radiation (λ=0.71073 Å). Reflections, measured at 293 K within a 2θ range of 1.55–26.99°, were corrected for background, Lorentz polarization, and absorption (μ=0.116 mm^{-1}), while crystal decay was negligible. The structure was solved by direct methods. For the structural refinement the non-hydrogen atoms were treated anisotropically, and the hydrogen atoms, included in the structure factor calculation, were refined isotropically. Final discrepancy indices were R_F=5.65% and R_W=13.08% using a unit weight for 2947 reflections and refining 306 parameters. The final difference Fourier map was essentially featureless, the highest residual peaks having densities of 0.164 e/A^3. Crystallographic data for **2a** have been deposited with the Cambridge Crystallographic Data Centre. Copies of the data can be obtained, free of charge, on application to The Director, CCDC, 12 Union Road, Cambridge CB2 1EZ, UK. Fax: +44 1223 336033 or e-mail: deposit@ccdc.cam.ac.uk.

*4.1.2.4.1. 2,3,4,-Tri-O-acetyl-6-deoxy-L-mannose 2,4-dinitrophenylhydrazone (**2b**)*
Yellow oil; IR ($CHCl_3$) ν_{max} 3559, 3363, 1748, 1619, 1594, 1526, 2511, 1425, 1372, 1342, 1312, 1246, 1138, 1063, 924 cm^{-1}; ORD (*c* 0.66, $CHCl_3$) $[\alpha]_{589}$ +14, $[\alpha]_{578}$ +14, $[\alpha]_{546}$ +17; ^1H NMR (300 MHz, $CDCl_3$) δ 11.10 (1H, s), 9.12 (1H, d, *J*=2.5 Hz), 8.37 (1H, dd, *J*=9.3, 2.5 Hz), 7.91 (1H, d, *J*=9.3 Hz), 7.43 (1H, br d, *J*=5.2 Hz), 5.79 (1H, dd, *J*=8.5, 1.9 Hz), 5.54 (1H, dd, *J*=8.5, 5.2 Hz), 5.11 (1H, dd, *J*=8.5, 1.9 Hz), 3.72 (1H, ddq, *J*=8.5, 6.1, 4.9 Hz), 2.81 (1H, d, *J*=4.9 Hz), 2.13, 2.12, 2.10 (3H each, 3s), 1.20 (3H, d, *J*=6.1 Hz); ^{13}C NMR (75.4 MHz, $CDCl_3$) δ 171.5, 170.0, 169.6, 144.6, 143.8, 139.0, 130.3, 129.9, 123.2, 116.7, 73.5, 69.8, 69.0, 65.2, 20.9, 20.8, 20.7, 19.1; FABMS *m/z* $[M+H]^+$ 471, $[M]^+$ 470, $[M-C_2H_3O_2]^+$ 411, $[M-C_2H_3O_2-2C_2H_4O_2]^+$ 291; HRFABMS *m/z* 471.1369 (calcd for $C_{18}H_{22}N_4O_{11}$+H, 471.1363).

*4.1.2.4.2. 1-(2,3,4-Tri-O-acetyl-6-deoxy-α-L-mannopyranosyl)-2-(2,4-dinitrophenyl)hydrazine (**2c**)*
Yellow oil; IR ($CHCl_3$) ν_{max} 3575, 3557, 1790, 1731, 1604, 1487, 1466, 1445, 1390, 1294, 1246, 1103, 1063, 975 cm^{-1}; ORD (*c* 0.15, $CHCl_3$) $[\alpha]_{589}$ −19, $[\alpha]_{578}$ −20, $[\alpha]_{546}$ −22; ^1H NMR (300 MHz, $CDCl_3$) δ 9.50 (1H, s), 9.11 (1H, d, *J*=2.5 Hz), 8.31 (1H, dd, *J*=9.3, 2.5 Hz), 7.66 (1H, d, *J*=9.3 Hz), 5.29 (1H, dd, *J*=7.1, 4.1 Hz), 5.26 (1H, dd, *J*=5.8, 4.1 Hz), 4.98 (1H, dd, *J*=5.8, 5.0 Hz), 4.72 (1H, dd, *J*=6.9, 5.0 Hz), 4.44 (1H, d, *J*=7.1 Hz), 4.11 (1H, quint, *J*=6.9 Hz), 2.15, 2.12, 2.09 (3H each, 3s), 1.36 (3H, d, *J*=6.9 Hz); ^{13}C NMR (75.4 MHz, $CDCl_3$) δ 169.9, 169.6, 169.6, 149.3, 137.5, 130.2, 129.7, 123.8, 115.4, 83.9, 71.1, 70.3, 68.9, 66.8, 20.9, 20.8, 20.7, 16.9; EIMS *m/z* (rel int.) $[M]^+$ 470 (1), 446 (1), 306 (9), 291 (11), 273 (14), 213 (5), 193 (5), 171 (11), 153 (41), 129 (8), 111 (33), 83 (11), $[C_2H_3O]^+$ 43 (100); HREIMS *m/z* 470.1273 $[M]^+$ (calcd for $C_{18}H_{22}N_4O_{11}$, 470.1285).

*4.1.2.4.3. 2,3,4,5-Tetra-O-acetyl-6-deoxy-L-mannose 2,4-dinitrophenylhydrazone (**3**)*
Yellow oil; IR ($CHCl_3$) ν_{max} 3309, 1746, 1619, 1594, 1509, 1437, 1373, 1340, 1235, 1147, 1062, 1038, 924, 837 cm^{-1}; ORD (*c* 1.14, $CHCl_3$) $[\alpha]_{589}$ −14, $[\alpha]_{578}$ −15, $[\alpha]_{546}$ −17; ^1H NMR (300 MHz, $CDCl_3$) δ 11.08 (1H, s), 9.12 (1H, d, *J*=2.5 Hz), 8.35 (1H, dd, *J*=9.5, 2.5 Hz), 7.96 (1H, d, *J*=9.5 Hz), 7.35 (1H, dd, *J*=6.0, 1.0 Hz), 5.58 (1H, dd, *J*=8.0, 3.0 Hz), 5.50 (1H, dd, *J*=8.0, 6.0 Hz), 5.36 (1H, dd, *J*=8.5, 3.0 Hz), 5.04 (1H, dq, *J*=8.5, 6.5 Hz), 2.12 (3H, s), 2.12 (3H, s), 2.06 (3H, s), 2.04 (3H, s), 1.24 (3H, d, *J*=6.5 Hz); ^{13}C NMR (75.4 MHz, $CDCl_3$) δ 169.9, 169.9, 169.8, 169.4, 144.6, 144.0, 138.9, 130.1, 129.8, 123.1, 116.7, 70.9, 69.8, 68.7, 66.8, 21.0, 20.7, 20.7, 20.6, 16.3; EIMS (20 eV) *m/z* (rel int.) $[M]^+$ 512 (0.1), $[M-C_2H_3O_2]^+$ 453 (1), $[453-2C_2H_4O_2]^+$ 333 (2), $[333-C_2H_2O]^+$ 291 (10), 290 (14), 251 (16), 129 (10), 117 (10), 111 (11), $[C_2H_3O]^+$ 43 (100); FABMS *m/z* $[M+Na]^+$ 535; HRFABMS *m/z* 535.1288 $[M+Na]^+$ (calcd for $C_{20}H_{24}N_4O_{12}$+Na 535.1286).

4.1.3. Molecular modeling calculations. Geometry optimizations were carried out using the MMFF94 force-field calculations as implemented in the Spartan'04 program.[23] The systematic conformational search for the pyranoside rings was achieved with the aid of Dreiding models considering torsion angle movements of ca. 30°. The E_{MMFF} values were used as the convergence criterion and a further search with the Monte Carlo protocol was carried without considering energy cut off. All local minima were geometry optimized by DFT at the B3LYP/6-31G(d) level using the Spartan'04 routines. The Altona equation was used to calculate vicinal couplings from dihedral angles for each conformer. Gaussian 03W[24] were used to calculate the ^{13}C NMR chemical shifts at the B3LYP/6-31G(d,p) level. The thermochemical parameters ΔE_0, ΔE_{298}, ΔH_{298}, and ΔS_{298} were calculated at the same level considering vibrational frequencies at 298.15 K and 1 atm. These values were used for

estimation of the relative populations according to the following equations: $\Delta G=\Delta H-T\Delta S$ and $\Delta G=-RT \ln K$.

Acknowledgements

This research was supported by grants from CONACyT (45759-Q) and DGAPA, UNAM (IN214205-2). We wish to thank Georgina Duarte and Margarita Guzmán (USAI, Facultad de Química, UNAM) for some of the mass spectra measurements. We are most grateful to Professor Tony Durst (Department of Chemistry, University of Ottawa) for providing facilities to record high-resolution mass spectra.

References and notes

1. Schmidt, E. W. *Hydrazine and Its Derivatives: Preparation, Properties, Applications*; Wiley: New York, NY, 2001; pp 150–155.
2. Ragnarsson, U.; Fransson, B.; Grehn, L. *J. Chem. Soc., Perkin Trans. 1* **2000**, 1405–1409.
3. Wilcox, C. F.; Bauer, S. H. *THEOCHEM* **2003**, *625*, 1–6.
4. Yamabe, S.; Ishikawa, T. *J. Org. Chem.* **1999**, *64*, 4519–4524.
5. Takeda, Y. *Carbohydr. Res.* **1979**, *77*, 9–23.
6. Williams, J. M. *Carbohydr. Res.* **1983**, *117*, 89–94.
7. Ojala, W. H.; Gleason, W. B. *Acta Crystallogr., Sect. C* **1996**, *52*, 3188–3190.
8. Furberg, S.; Solbakk, J. *Acta Chem. Scand.* **1969**, *23*, 3248–3256.
9. Blair, H. S.; Roberts, G. A. F. *J. Chem. Soc. C* **1967**, *22*, 2425–2427.
10. Somogy, L. *Carbohydr. Res.* **1978**, *64*, 289–292.
11. Pereda-Miranda, R.; Fragoso-Serrano, M.; Cerda-García-Rojas, C. M. *Tetrahedron* **2001**, *57*, 47–53.
12. Fragoso-Serrano, M.; Guillén-Jaramillo, G.; Pereda-Miranda, R.; Cerda-García-Rojas, C. M. *J. Org. Chem.* **2003**, *68*, 7167–7175.
13. Becke, A. D. *Phys. Rev. A* **1988**, *38*, 3098–3100.
14. Da Silva, C. O.; Mennucci, B.; Vreven, T. *J. Org. Chem.* **2004**, *69*, 8161–8164.
15. Thibaudeau, C.; Stenutz, R.; Hertz, B.; Klepach, T.; Zhao, S.; Wu, Q.; Carmichael, I.; Serianni, A. S. *J. Am. Chem. Soc.* **2004**, *126*, 15668–15685.
16. Tvaroska, I.; Taravel, F. R.; Utille, J. P.; Carver, J. P. *Carbohydr. Res.* **2002**, *337*, 353–367.
17. Makowski, M.; Chmurzynski, L. *THEOCHEM* **2002**, *579*, 247–256.
18. Domínguez, J. A. *J. Am. Chem. Soc.* **1951**, *73*, 849.
19. Chang, G.; Guida, W. C.; Still, W. C. *J. Am. Chem. Soc.* **1989**, *111*, 4379–4386.
20. Cremer, D.; Pople, J. A. *J. Am. Chem. Soc.* **1975**, *97*, 1354–1358.
21. Haasnoot, C. A. G.; de Leeuw, F. A. A. M.; Altona, C. *Tetrahedron* **1980**, *36*, 2783–2792.
22. Smiataczowa, K.; Maj, K.; Skurski, P. *Eur J. Org. Chem.* **2001**, 4269–4274.
23. Kong, J.; White, C. A.; Krylov, A. I.; Sherrill, C. D.; Adamson, R. D.; Furlani, T. R.; Lee, M. S.; Lee, A. M.; Gwaltney, S. R.; Adams, T. R.; Ochsenfeld, C.; Gilbert, A. T. B.; Kedziora, G. S.; Rassolov, V. A.; Maurice, D. R.; Nair, N.; Shao, Y.; Besley, N. A.; Maslen, P. E.; Dombroski, J. P.; Daschel, H.; Zhang, W.; Korambath, P. P.; Baker, J.; Byrd, E. F. C.; Van Voorhis, T.; Oumi, M.; Hirata, S.; Hsu, C. P.; Ishikawa, N.; Florian, J.; Warshel, A.; Johnson, B. G.; Gill, P. M. W.; Head-Gordon, M.; Pople, J. A. *J. Comput. Chem.* **2000**, *21*, 1532–1548.
24. Frisch, M. J.; Trucks, G. W.; Schlegel, H. B.; Scuseria, G. E.; Robb, M. A.; Cheeseman, J. R.; Montgomery, J. A., Jr.; Vreven, T.; Kudin, K. N.; Burant, J. C.; Millam, J. M.; Iyengar, S. S.; Tomasi, J.; Barone, V.; Mennucci, B.; Cossi, M.; Scalmani, G.; Rega, N.; Petersson, G. A.; Nakatsuji, H.; Hada, M.; Ehara, M.; Toyota, K.; Fukuda, R.; Hasegawa, J.; Ishida, M.; Nakajima, T.; Honda, Y.; Kitao, O.; Nakai, H.; Klene, M.; Li, X.; Knox, J. E.; Hratchian, H. P.; Cross, J. B.; Bakken, V.; Adamo, C.; Jaramillo, J.; Gomperts, R.; Stratmann, R. E.; Yazyev, O.; Austin, A. J.; Cammi, R.; Pomelli, C.; Ochterski, J. W.; Ayala, P. Y.; Morokuma, K.; Voth, G. A.; Salvador, P.; Dannenberg, J. J.; Zakrzewski, V. G.; Dapprich, S.; Daniels, A. D.; Strain, M. C.; Farkas, O.; Malick, D. K.; Rabuck, A. D.; Raghavachari, K.; Foresman, J. B.; Ortiz, J. V.; Cui, Q.; Baboul, A. G.; Clifford, S.; Cioslowski, J.; Stefanov, B. B.; Liu, G.; Liashenko, A.; Piskorz, P.; Komaromi, I.; Martin, R. L.; Fox, D. J.; Keith, T.; Al-Laham, M. A.; Peng, C. Y.; Nanayakkara, A.; Challacombe, M.; Gill, P. M. W.; Johnson, B.; Chen, W.; Wong, M. W.; Gonzalez, C.; Pople, J. A.; Gaussian 03, revision C.02: Wallingford, CT, 2004.